GEOPHYSICAL RESEARCH LETTERS, VOL. 32, L05611, doi:10.1029/2004GL021745, 2005

# Climatological annual cycle of upper ocean oxygen content anomaly

Hernan E. Garcia, Tim P. Boyer, Sydney Levitus, Ricardo A. Locarnini, and John I. Antonov

National Oceanographic Data Center, NOAA, Silver Spring, Maryland, USA

Received 13 October 2004; revised 24 January 2005; accepted 9 February 2005; published 10 March 2005.

[1] The climatological annual cycle of oxygen content anomaly of the 0–100 m depth layer for major ocean basins is described using Fourier analysis of objectively analyzed monthly $O_2$ anomaly values on a 1° grid (70°S–70°N). The largest seasonal changes in $O_2$ content anomaly occur in the extra-tropics in the 30° to 60° latitude belt of each hemisphere. The magnitude of the global cycle is dominated by the Pacific Ocean. The annual and semi-annual harmonics account for most (>90%) of the annual cycle of the monthly $O_2$ content anomaly. The magnitude of the annual harmonic is largest in the upper 75 m layer except in the tropics and high latitudes. The annual harmonic accounts for >90% of the variance of the zonally integrated monthly $O_2$ content anomaly. **Citation:** Garcia, H. E., T. P. Boyer, S. Levitus, R. A. Locarnini, and J. I. Antonov (2005), Climatological annual cycle of upper ocean oxygen content anomaly, *Geophys. Res. Lett.*, *32*, L05611, doi:10.1029/2004GL021745.

## 1. Introduction

[2] Dissolved oxygen plays a central role in most ocean biogeochemical processes throughout the water column, the air-sea interface, and the sediments. Its concentration is maintained by physical and biochemical processes such as air-sea gas exchange, photosynthesis and respiration, bubble mediated gas exchange, equilibration time, and by water mass mixing. The $O_2$ concentration is also affected by temperature variability through its effect on the solubility of $O_2$ in seawater and by the effect of vertical stratification and mixing on biological production (biophysical forcing). Identifying changes in the annual $O_2$ cycle has important implications for understanding climate variability [*Emerson et al.*, 2001; *Keeling and Garcia*, 2002; *Plattner et al.*, 2002; *Matear et al.*, 2000; *Sarmiento et al.*, 1998; *Bopp et al.*, 2002]. Global ocean baseline estimates of the seasonal $O_2$ content are required for understanding variability in the partition of $O_2$ within the ocean and between the ocean and the atmosphere.

[3] We present a quantitative description of the observation-based climatological annual cycle of ocean $O_2$ content anomaly in the upper 100 m depth of the water column on global and basin scales. The upper 100 m depth of the water column was chosen to represent the oceanic surface layer most directly affected by seasonal atmospheric and primary production processes. A global and basin approach allows comparison of regional differences and phasing of the seasonal $O_2$ cycle in the context of global climate scales which can be used as constraints for seasonally resolved biophysical models. Previous studies of the seasonal distribution of $O_2$ have been confined to limited geographic regions [*Jenkins and Goldman*, 1985; *Emerson*, 1987; *Spitzer and Jenkins*, 1989; *Craig and Hayward*, 1987], the near surface ocean [*Najjar and Keeling*, 1997], or limited to seasonal differences [*Boyer et al.*, 1999].

## 2. Methods

[4] We use monthly objectively analyzed $O_2$ fields on a 1° grid at 0, 10, 20, 30, 50, 75, and 100 m depth to compute the monthly $O_2$ content anomaly ($OC_m$) for each 1° × 1° grid box between 70°S and 70°N using,

$$OC_m = A \int_{z_1}^{z_2} \Delta O_2 dz$$

where A is the area ($m^2$) of each 1° × 1° grid box calculated assuming an earth radius of 6378 km, $\Delta O_2$ ($\mu mol\ m^{-3}$) is the monthly minus the annual climatological $O_2$ value, and dz (m) is the vertical thickness (m) of each depth layer taken to be the difference between adjacent depths $z_1$ and $z_2$. The zonal and basin $OC_m$ are defined then as the sum of $OC_m$ estimates by 1° latitude belts. *Boyer et al.* [2002] describe the objective analysis technique and *Locarnini et al.* [2002a, 2002b] describe the monthly $O_2$ mean fields of the *World Ocean Atlas 2001* (*WOA01*). The *WOA01* $O_2$ fields were converted from units of ml $l^{-1}$ to $\mu mol\ m^{-3}$ using a molar volume of $O_2$ of 22.4l.

## 3. Basin Zonal $O_2$ Content

[5] We begin by describing the annual cycle of the zonal integral of $OC_m$ by 1° latitude bands for the world ocean. The largest seasonal changes occur in the extra-tropics in the 30° to 60° latitude belt of the Northern (NH) and Southern (SH) Hemispheres (Figure 1). In the SH, the largest seasonal changes occur in the latitudinal band centered near 40°S. The March to May $OC_m$ peak is slightly larger in magnitude (∼−3.2 Tmol; 1 Tmol = $10^{12}$ mol) than during August to December (∼2.6 Tmol). But the March to May peak spans a shorter duration compared to the August to December peak. The transition between seasonal increases and decreases in $OC_m$ occurs approximately in July. The situation is roughly reversed in the extra-tropical NH as the two hemispheres are nearly 6 months out of phase. $OC_m$ values decrease poleward of 60° latitude. This may simply be due to the decrease of ocean volume with increasing latitude. In addition, this might also be an artifact due to lack of $O_2$ data coverage in the high latitudes and/or the patchy nature of biological production. In the tropics


0094-8276/05/2004GL021745$05.00

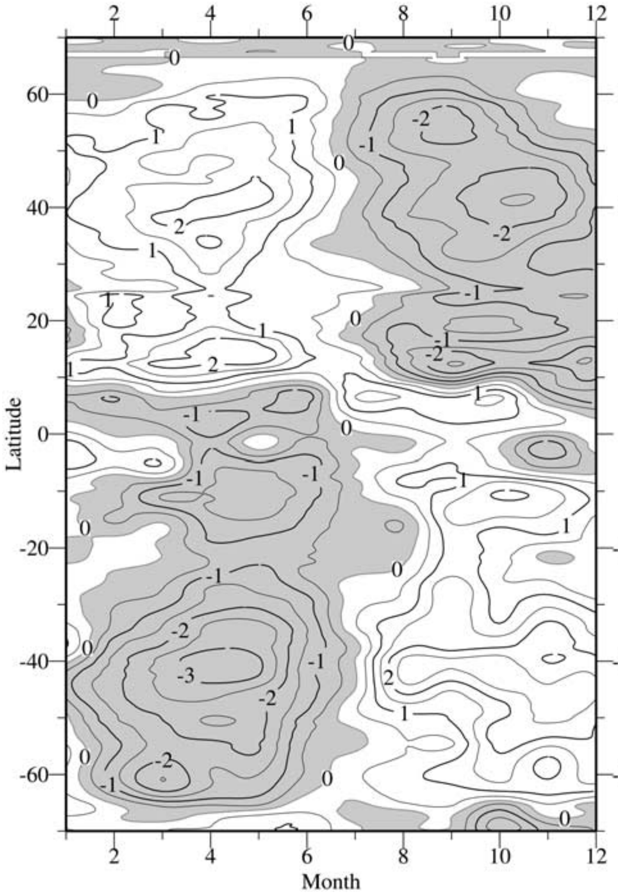


**Figure 1.** Zonally integrated monthly $O_2$ content anomaly of the 0 to 100 m depth layer for the World Ocean. Shading denotes negative values. The contour interval is 0.5 Tmol (1 Tmol = $10^{12}$ mol).

(10°S–10°N), $OC_m$ values are small compared to the extra-tropics (>20°). The 10°S–10°N band is predominantly in phase with the SH annual cycle and can be nominally regarded as being part of, or in phase with, the SH seasonal $O_2$ regime consistent with the approximate region of the

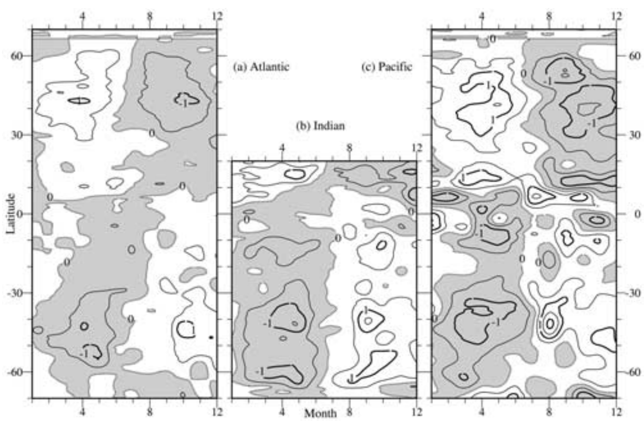


**Figure 2.** Zonally integrated monthly $O_2$ content anomaly of the 0 to 100 m depth layer for the (a) Atlantic, (b) Indian, and (c) Pacific Basins. Shading denotes negative values. The contour interval is 0.5 Tmol (1 Tmol = $10^{12}$ mol).

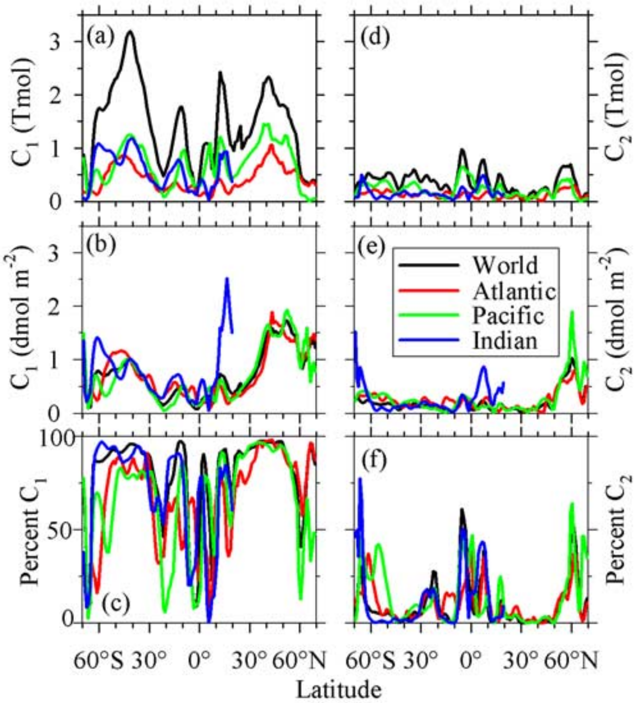


**Figure 3.** Amplitude and percent variance accounted for by the annual ($C_1$) [3a-c] and semi-annual ($C_2$) [3d-g] harmonics of the zonally integrated $O_2$ content anomaly as a function of latitude for the 0 to 100 m depth layer for the major ocean basins based on the *WOA01*.

Intertropical Convergence Zone (ITCZ). Figure 2 illustrates that all major ocean basins exhibit similar distributions of the zonally integrated $OC_m$.

[6] We performed a Fourier analysis of the zonally integrated $OC_m$ to quantify the amplitude and timing of the $O_2$ annual cycle (Figure 3). The amplitude of the annual ($C_1$) and semi-annual ($C_2$) harmonics account for most of

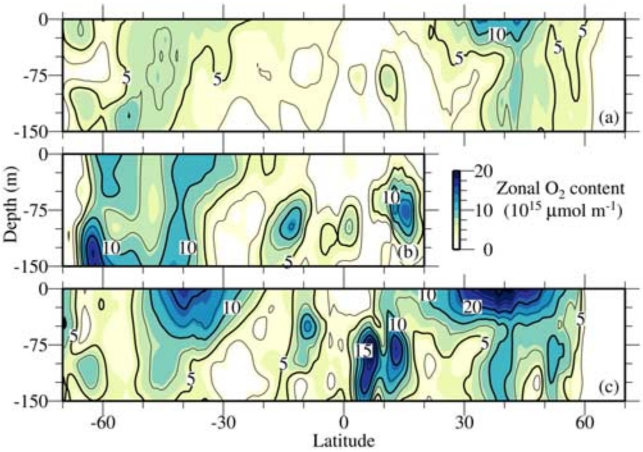


**Figure 4.** Amplitude of the annual harmonic of the zonally integrated monthly $O_2$ content anomaly per unit meter of depth for (a) Atlantic, (b) Indian, and (c) Pacific Basins. Zonal $O_2$ content anomaly values have been multiplied by the area of each zonal band of each basin. The contour interval is $2.5 \times 10^{15}$ μmol $m^{-1}$.

**Table 1.** Fourier Parameters (Amplitude, Phase, and Percent Variance) and Positive Seasonal Oxygen Content (PSOC) Anomaly Estimates Using the Annual Harmonic of the Monthly Zonal Oxygen Content Anomaly for the 0 to 100 m Depth Layer for Major Ocean Basins

| Basin | Amplitude ($10^{20}$ μmol) | Phase (month) | Variance (%) | PSOC (mol $m^{-2}$) | Area ($10^{14}$ $m^2$) |
|---|---|---|---|---|---|
| N. Atlantic (0°–70°N) | 0.29 | 3.7 | 97.4 | 2.5 | 0.44 |
| N. Pacific (0°–70°N) | 0.42 | 3.9 | 96.2 | 2.0 | 0.79 |
| N. Indian (0°–25°N) | 0.57 | 3.8 | 88.4 | 19.8 | 0.11 |
| N. Hemisphere (0°–70°N) | 0.79 | 3.8 | 97.7 | 2.3 | 1.33 |
| N. Hemisphere (20°–70°N) | 0.66 | 3.6 | 98.6 | 3.7 | 0.70 |
| S. Atlantic (0°–70°S) | 0.26 | 10.6 | 96.6 | 2.3 | 0.44 |
| S. Pacific (0°–70°S) | 0.36 | 10.0 | 91.3 | 1.5 | 0.94 |
| S. Indian (0°–70°S) | 0.42 | 9.7 | 96.5 | 2.7 | 0.62 |
| S. Hemisphere (0°–70°S) | 1.03 | 10.0 | 97.6 | 2.0 | 2.00 |
| S. Hemisphere (20°–70°S) | 0.84 | 9.9 | 96.9 | 2.4 | 1.35 |

the variance of the latitudinal variations of the zonally integrated $OC_m$ values (Figures 3c and 3f). Between about 25° and 65° latitude, $C_1$ accounts for most (~90%) of the variance of the zonally integrated $OC_m$ values (Figure 3c). $C_2$ accounts for a greater percentage of the variance than $C_1$ in the region 25°S–25°N and the high latitudes near 60°N and 65°S (Figure 3f). The $C_2$ pattern in equatorial regions is consistent with a semi-annual signal in part due to the well-known semi-annual vertical displacements of the thermocline and in large regions of the Indian Ocean [*Levitus and Antonov*, 1997]. Poleward of 65°, the *WOA01* includes $O_2$ data sparse regions, particularly during winter making it difficult to assess the contribution to the variance of $C_2$ or higher harmonics. When compared to the global zonal integral of $OC_m$ on a per mole basis (volume integral), the Pacific Basin generally dominates the amplitude of both $C_1$ and $C_2$ with some exceptions (Figure 3a). South of 15°S, both the Indian and Pacific are the most important contributors to the zonally integrated $OC_m$. Figure 3b illustrates that all basins exhibit similar estimates of zonally integrated $OC_m$ on a mole per unit area except the North Indian Basin.

[7] The amplitude of $C_1$ reveals several peaks most notably located near 42°S (~3.2 Tmol), 11°S (~1.8 Tmol), 5°N (~1.1 Tmol), 10°N (~2.4 Tmol), and 45°N (~2.3 Tmol) in the major basins (Figure 3a). The peaks within the tropics are associated with the system of equatorial currents and counter-currents (Figure 4). The equatorial region is subject to intense upwelling of under-saturated $O_2$ waters and to transient forcing such as El Niño. We note that the geographical locations of the $C_1$ peaks are close to those for heat content [*Antonov et al.*, 2004]. This suggests a strong correlation between $O_2$ and heat content due to the effect of dynamical and biological processes. The amplitude of $C_1$ is generally largest in the upper 75 m layer (Figure 4). All the major basins show similar zonally integrated $OC_m$ per unit area except poleward of about 10°N in the North Indian Ocean (Figures 3b and 3e). In summary, our results show that (1) both $C_1$ and $C_2$ are needed to account for most (>90%) of the large-scale latitudinal changes in zonally integrated $OC_m$ and that (2) the $OC_m$ signal is primarily surface forced.

[8] Fourier analysis of the zonally integrated $OC_m$ values indicates that $C_1$ accounts for >85% of the variance in all basins (Table 1). The North Indian Basin is affected by the southwest and northeast Monsoon winds that typically occur during boreal summer and winter respectively, as well as by upwelling. On hemispheric scales, $C_2$ plays a relatively smaller role compared to the amplitude of $C_1$, and thus, $C_1$ approximates well the $OC_m$ cycle in all major basins (Figure S1[1]). We note that the $C_1$ amplitude per unit area is slightly greater in the SH than in the NH (Table 1).

[9] Each basin can be expected to exhibit biological and physical sources and sinks of $O_2$ during the annual cycle. One way to compare basin-scale changes in $OC_m$ is by spatially integrating these estimates over the months when the spatially integrated $OC_m$ is positive. We term this estimate Positive Seasonal Oxygen Content (PSOC) anomaly. While PSOC values represent the net cumulative positive changes in $OC_m$ over the annual cycle irrespective of whether the integrated $OC_m$ is mediated by biological or physical sources, the remainder of the annual cycle represents net cumulative sinks of $OC_m$. Table 1 lists estimated PSOC values for all basins indicating that the NH has a slightly larger PSOC value than the SH (2.3 compared to 2.0 mol $m^{-2}$). The North Indian Ocean (0–25°N) has the largest PSOC value, ~20 mol $m^{-2}$. The extra-tropical (20°–70° latitude) PSOC values are equivalent to $OC_m$ changes of roughly 36 (NH) and 23 (SH) μmol $kg^{-1}$ if spread evenly over the top 100 m of the water column of each hemisphere. Each basin reveals similar PSOC values poleward of about 20° suggesting common biophysical mechanisms. A strong relation between $O_2$ and heat content is expected in part because the $O_2$ solubility content is inversely correlated to the seasonal pattern of heating and cooling of the mixed layer, particularly in the extra-tropics (25°–65°). Oceanic regions of net heating and cooling are expected to result in sea-to-air and air-to-sea $O_2$ gas exchange respectively [*Najjar and Keeling*, 2000; *Garcia and Keeling*, 2001]. The magnitude of the changes in $OC_m$ is expected to be relatively large in oceanic regions where the effect of heat storage on $O_2$ solubility ($O_s$), biological $O_2$ production, and mixing is large compared to the annual mean conditions. For example, changes in $OC_m$ can be expected to be large during annual periods of high primary production, high $O_s$, and shoaling mixed layer. It is difficult to quantify the net contribution of biological $O_2$ production and mixing to the changes in $OC_m$. The $O_s$ contribution to $O_2$ can be estimated by calculating Apparent Oxygen Utilization (AOU = $O_s - O_2$). $O_s$ values assume complete $O_2$ equilibration with the atmosphere. Figure S2 shows that a large fraction of the extra-tropical $C_1$ $OC_m$ is associated with seasonal $O_s$ content variability. The $O_s$ content anomaly due to temperature, while reflected in the amplitude of

[1]Auxiliary material is available at ftp://ftp.agu.org/apend/gl/2004GL021745.

$C_1$ is not as pronounced in other geographic regions such as the North Indian Ocean, Bering Sea, the Peru-Chile coastal region, the eastern equatorial Pacific, and portions of the Southern Ocean. Given the strong extra-tropical correlation between heat and $O_2$ content, future studies should take into account the difference in timing between their annual cycles.

## 4. Summary

[10] The global ocean annual cycle of $OC_m$ in the 0–100 m layer for major basins is described. The largest seasonal changes in $OC_m$ in this layer occur in the extra-tropics in the 30° to 60° latitude belt of each hemisphere. The magnitude of the global $OC_m$ cycle is dominated by the Pacific Ocean. Fourier analysis indicates that the annual and semi-annual harmonics account for most of the variance of the zonal integral of $OC_m$. While the annual harmonic accounts for most (>90%) of the variance in the extra-tropics, the semi-annual harmonic becomes important in the tropics. The annual amplitude of the global $OC_m$ per unit area is estimated to be 0.6 (NH) and 0.5 (SH) mol $m^{-2}$. The annual $OC_m$ signal is subject to uncertainty resulting from sampling errors, variability, sampling density, and other factors which are difficult to quantify. We believe that the $OC_m$ cycle is representative of the mean large-scale seasonal time scale. With presently available data, these global ocean results are expected to be useful constraints on global seasonally resolved biophysical models. Additional high-quality $O_2$ data will likely improve the results and help provide constraints on the seasonal $O_2$ content cycle, particularly in the extra-tropical Southern Hemisphere. For example, $O_2$ sensors have been deployed on ARGO floats and other instruments which have the potential to mitigate lack of temporal and spatial availability of $O_2$ data [*Emerson et al.*, 2002; *Körtzinger et al.*, 2004]. Because oceanic heat content variability is expected to affect vertical stratification, it is important to understand the biophysical implications of seasonal and longer time-scale variability in $O_2$ content.

[11] **Acknowledgments.** We thank the scientists, technicians, data center staff and managers for their contributions of data to the World Data Center system which has allowed us to compile the database used in this work. We thank our colleagues at the Ocean Climate Laboratory for their work in constructing the *World Ocean Database* which made this work possible. We also thank two anonymous reviewers for constructive comments. The views, opinions, and findings contained in this report are those of the authors, and should not be construed as an official NOAA or U.S. Government position, policy, or decision.

## References

Antonov, J. I., S. Levitus, and T. P. Boyer (2004), Climatological annual cycle of ocean heat content, *Geophys. Res. Lett.*, *31*, L04304, doi:10.1029/2003GL018851.

Bopp, L., C. Le Quéré, M. Heimann, A. C. Manning, and P. Monfray (2002), Climate-induced oceanic oxygen fluxes: Implications for the contemporary carbon budget, *Global Biogeochem. Cycles*, *16*(2), 1022, doi:10.1029/2001GB001445.

Boyer, T. P., M. Conkright, and S. Levitus (1999), Seasonal variability of dissolved oxygen and percent oxygen saturation in the Atlantic and Pacific Oceans, *Deep Sea Res.*, *46*, 1593–1613.

Boyer, T. P., C. Stephens, J. I. Antonov, M. E. Conkright, R. A. Locarnini, T. D. O'Brien, H. E. and Garcia (2002), *World Ocean Atlas 2001*, vol. 2, *Salinity*, *NOAA Atlas NESDIS*, vol. 50, edited by S. Levitus, 165 pp., U.S. Govt. Print. Off., Washington, D. C.

Craig, H., and T. Hayward (1987), Oxygen supersaturation in the ocean: Biological versus physical contributions, *Science*, *235*, 199–202.

Emerson, S. (1987), Seasonal oxygen cycles and biological new production in surface waters of the subarctic Pacific Ocean, *J. Geophys. Res.*, *92*, 6335–6544.

Emerson, S., S. Mecking, and J. Abell (2001), The biological pump in the subtropical North Pacific Ocean: Nutrient sources, Redfield Ratios, and recent changes, *Global Biogeochem. Cycles*, *15*, 535–554.

Emerson, S., C. Stump, B. Johnson, and D. M. Karl (2002), In-situ determination of oxygen and nitrogen dynamics in the upper ocean, *Deep Sea Res., Part I*, *49*, 941–952.

Garcia, H. E., and R. F. Keeling (2001), On the global oxygen anomaly and air-sea flux, *J. Geophys. Res.*, *106*, 31,155–31,166.

Jenkins, W. J., and W. B. Goldman (1985), Seasonal oxygen cycling and primary production in the Sargasso Sea, *J. Mar. Res.*, *43*, 465–491.

Keeling, R., and H. Garcia (2002), The change in oceanic $O_2$ inventory associated with recent global warming, *Proc. U.S. Natl. Acad. Sci.*, *99*, 7848–7853.

Körtzinger, A., J. Schimanski, U. Send, and D. Wallace (2004), The ocean takes a deep breath, *Science*, *306*, 1337.

Levitus, S., and J. Antonov (1997), *Climatological and Interannual Variability of Temperature, Heat Storage, and Rate of Heat Storage in the Upper Ocean, NOAA NESDIS Atlas*, vol. 16, 6 pp., 186 figures, U.S. Govt. Print. Off., Washington, D. C.

Locarnini, R. A., T. D. O'Brien, H. E. Garcia, J. I. Antonov, T. P. Boyer, M. E. Conkright, and C. Stephens (2002a), *World Ocean Atlas 2001*, vol. 3, *Oxygen*, *NOAA Atlas NESDIS*, vol. 51, edited by S. Levitus, 286 pp., U.S. Govt. Print. Off., Washington, D. C.

Locarnini, R. A., et al. (2002b), *World Ocean Database 2001*, vol. 4, *Temporal Distribution of Temperature, Salinity, and Oxygen Profiles, NOAA Atlas NESDIS*, vol. 45, edited by S. Levitus, 233 pp., U.S. Govt. Print. Off., Washington, D. C.

Matear, R. J., A. C. Hirst, and B. I. McNeil (2000), Changes in dissolved oxygen in the Southern Ocean with climate change, *Geochem. Geophys. Geosyst.*, *1*(11), doi:10.1029/2000GC000086.

Najjar, R., and R. Keeling (1997), Analysis of the mean annual cycle of the dissolved oxygen anomaly in the world ocean, *J. Mar. Res.*, *55*, 117–151.

Najjar, R., and R. Keeling (2000), Mean annual cycle of the air-sea oxygen flux: A Global view, *Global Biochem. Cycles*, *14*, 573–584.

Plattner, G., F. Joos, and T. F. Stocker (2002), Revision of the global carbon budget due to changing air-sea oxygen fluxes, *Global Biogeochem. Cycles*, *16*(4), 1096, doi:10.1029/2001GB001746.

Sarmiento, J. L., T. M. C. Hughes, R. J. Stouffer, and S. Manabe (1998), Simulated response of the ocean carbon cycle to anthropogenic climate warming, *Nature*, *393*, 245–249.

Spitzer, W. S., and W. J. Jenkins (1989), Rates of vertical mixing, gas exchange and new production: Estimates from seasonal gas cycles in the upper ocean near Bermuda, *J. Mar. Res.*, *47*, 169–196.

J. I. Antonov, T. P. Boyer, H. E. Garcia, S. Levitus, and R. A. Locarnini, NESDIS/NOAA, National Oceanographic Data Center, E/OC5, 1315 East-West Highway, Silver Spring, MD, USA. (hernan.garcia@noaa.gov)

**Auxiliary Material Submission for Paper**
2004GL021745,
Climatological Annual Cycle of Ocean Oxygen Content Anomaly H.E. Garcia, T.P. Boyer, S. Levitus, R.A. Locarnini, and J.I. Antonov (Ocean Climate Laboratory, National Oceanographic Data Center/NOAA, Silver Spring MD)
Geophysical Research Letters

Introduction: This supplementary material contains two figures (2004gl021745-FigureS1.eps and 2004gl021745-FigureS2.eps). These figures provide information on spatially integrated monthly oxygen content anomalies and the amplitude of the annual harmonic of the monthly oxygen and apparent oxygen utilization content (AOU) based on the World Ocean Atlas 2001 (WOA01). For more information about the WOA01, see http://www.nodc.noaa.gov/OCL/indprod.html.

2004gl021745-FigureS1 figure caption:
Figure S1. Zonally integrated monthly oxygen content anomaly of the 0 to 100 m depth layer in the Northern (black line) and Southern (dashed black line) Hemispheres. Also shown is the oxygen content anomaly based on the annual harmonic in the Northern (red line) and Southern (dashed red line) Hemispheres.

2004gl021745-FigureS2 figure caption:
Figure S2. Amplitude per unit area of the annual harmonic for the 0-100 m depth of the monthly content anomaly of (a) oxygen and (b) Apparent Oxygen Utilization (AOU). The contour interval is 1 mol per squared meter.

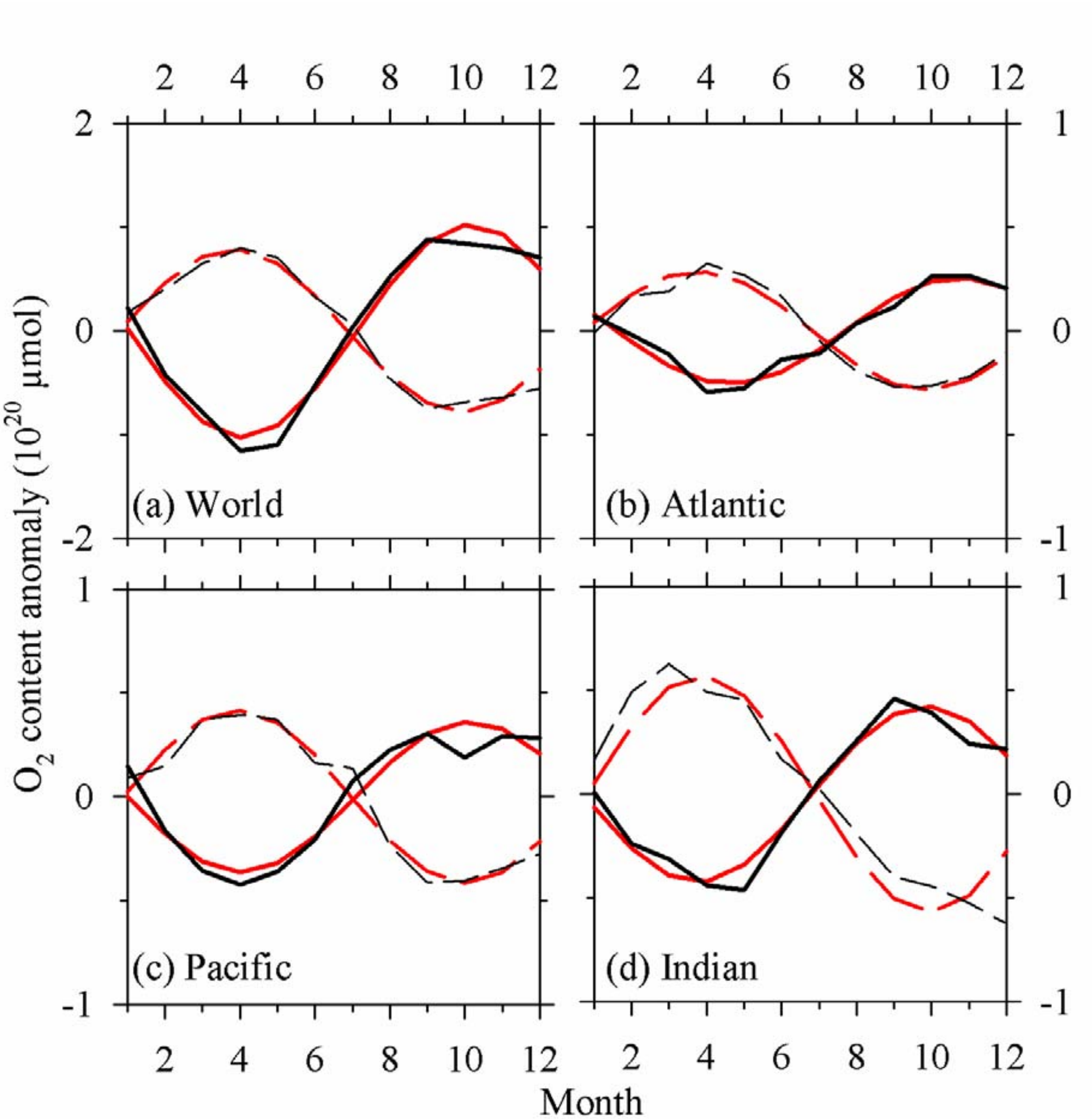


**Figure S1.** Zonally integrated monthly oxygen content anomaly of the 0 to 100 m depth layer in the Northern (black line) and Southern (dashed black line) Hemispheres. Also shown is the oxygen content anomaly based on the annual harmonic in the Northern (red line) and Southern (dashed red line) Hemispheres.

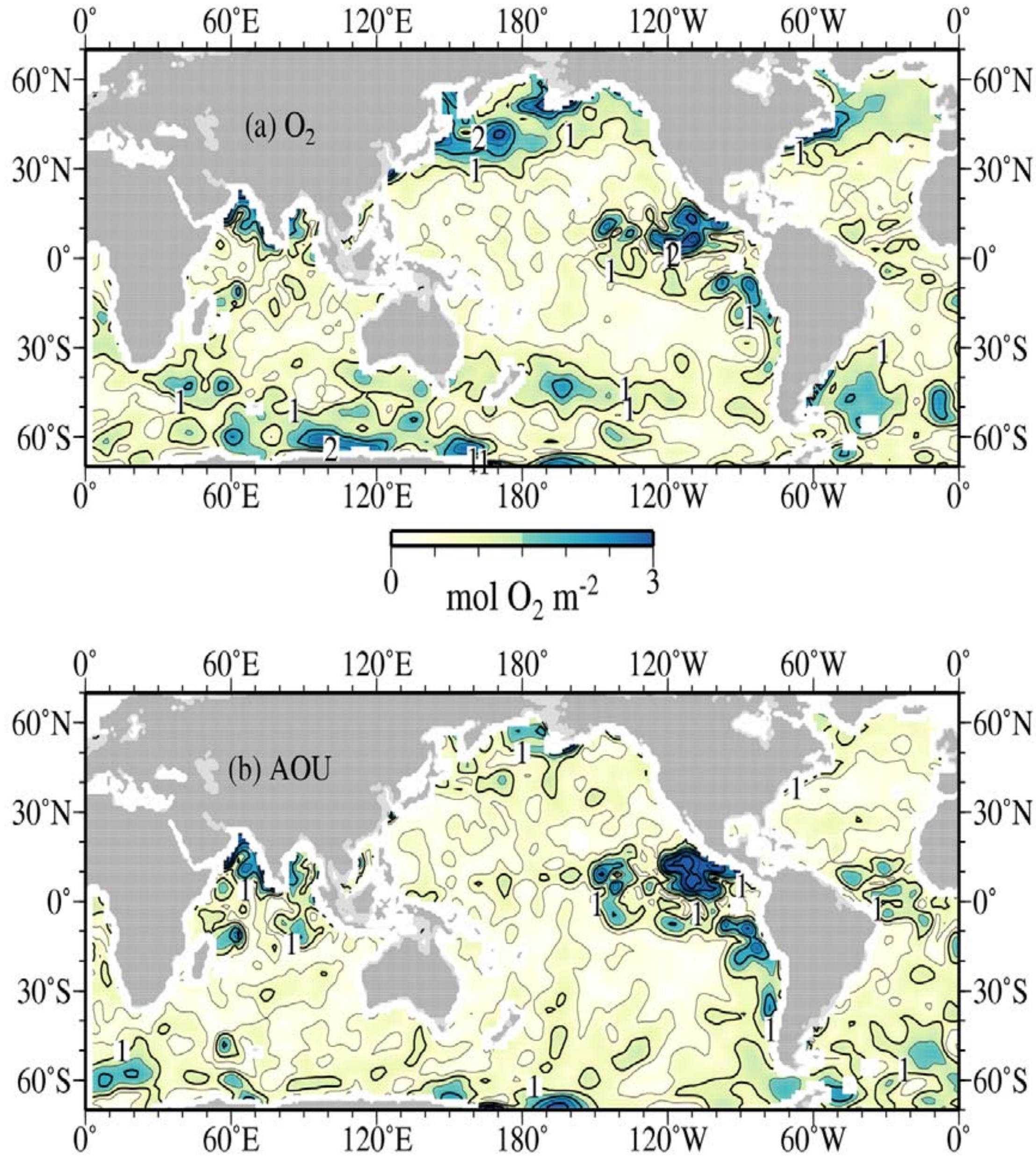


**Figure S2.** Amplitude per unit area of the annual harmonic for the 0-100 m depth of the monthly content anomaly of (a) oxygen and (b) Apparent Oxygen Utilization (AOU). The contour interval is 1 mol per squared meter.